doi: 10.82124/CEAS-GNC-2026-057 CEAS-GNC-2026-057

EuroGNC CEAS Madrid, Spain May 5th-7th 2026

Impact of Model Fidelity on Load and State Estimation in Hybrid Observers Using Wind Tunnel Data

O. Luderer Research Engineer, Institute of Aircraft Systems Engineering, Hamburg University of Technology, Nesspriel 5, 21129 Hamburg, Germany. oliver.luderer@tuhh.de

L. Rieck Research Engineer, Institute of Aircraft Systems Engineering, Hamburg University of Technology, Nesspriel 5, 21129 Hamburg, Germany. leif.rieck@tuhh.de

B. Herrmann Research Engineer, Institute of Aircraft Systems Engineering, Hamburg University of Technology, Nesspriel 5, 21129 Hamburg, Germany. benjamin.herrmann@tuhh.de

F. Thielecke Professor, Institute of Aircraft Systems Engineering, Hamburg University of Technology, Nesspriel 5, 21129 Hamburg, Germany. frank.thielecke@tuhh.de

ABSTRACT

The hybrid load observer used for structural load monitoring combines a physical load observer based on a flight-dynamics model with a data-driven correction model. This correction model enables precise load estimation even under physical model uncertainties and neglected physical effects. As such, it is effective in cases where the physical model structure is not immediately apparent and complements purely physics-based modeling approaches, without neglecting the underlying physics. In this sense, the hybrid load observer may serve as a model-based source of essential load information required for modern load alleviation concepts. Besides load estimates, other quantities, such as aeroelastic states, are often relevant for flexible aircraft control. However, these have hardly been considered in previous applications of the hybrid load observer, as it has so far only been applied for load monitoring. Thus, the impact of underlying model uncertainties on crucial states for load control (e.g. aeroelastic states) remains pending. This open aspect is examined in the present work in more detail using wind tunnel data of a flexible wing and by explicitly accounting for physical model uncertainties. To this end, the hybrid load observer, based on an unvalidated design model, is compared with a conventional observer without a correction model that relies on a refined physical model derived from test data. Both physical load observers are based on an LPV extended Kalman filter. The advantages of using a correction model for load estimation are demonstrated in a direct comparison of both observers. Specifically, the hybrid load observer achieves a better load estimation result than the refined LPV extended Kalman filter despite its reduced physical model fidelity. However, the comparison also reveals the shortcomings of the hybrid load observer's current formulation, as model uncertainties affect the quality of the estimated structural dynamic modes and are not yet sufficiently corrected by the correction model.

Keywords: Load Estimation, State Estimation, Hybrid Observer, Linear Parameter-Varying System

Nomenclature

f = Frequency
k = k-factor
$p_{\mathrm{max}}, p_{\mathrm{min}}$ = Maximum and minimum measured angular rate
$q, \dot{q}$ = Body-fixed pitch rate and derivative
r = Residuum
$u, w, \dot{u}, \dot{w}$ = Body-fixed velocities / accelerations
$u_{\mathrm{P}}, u_{\mathrm{LMN}}$ = Input vector
$\hat{\tilde{u}}$ = Input vector in deviation coordinates
w = Weighting factor
$\hat{x}_k^-, \hat{x}_k$ = A priori and a posteriori state estimates
$\tilde{x}, \hat{\tilde{x}}$ = State vector in deviation coordinates
$\Delta\hat{x}_{\mathrm{s}}$ = State correction
y_{L}, y_{s} = Measured Load / flight dynamics outputs
$\hat{y}_{\mathrm{L}}$, $\hat{y}_{\mathrm{s}}$ = Estimated Load / flight dynamics outputs
$\hat{y}_{\mathrm{L,EKF}}$ = Extended Kalman filter load estimate
$\hat{y}_{\mathrm{L,Hyb}}$ = Hybrid load observer load estimate
$\bar{x}, \bar{y}$ = Linearized equilibrium (trim) point
$\Delta\hat{y}_{\mathrm{L,LMN}}$ = Correction model load estimate
z_{W} = Disturbance
A, B, C, D = State-space matrices
C^{L}, D^{L} = State-space matrices containing only load outputs
C_{L}, C_{L0} = Lift / Zero-lift coefficient
$C_{\mathrm{L}\alpha}$ = Lift slope
C_{D}, C_{D0} = Drag / Zero-drag coefficient
F_η = Aerodynamic forces
$\mathrm{LS}_{\mathrm{I1}}$ - $\mathrm{LS}_{\mathrm{I5}}$ = IMU station
$\mathrm{LS}_{\mathrm{S1}}$ - $\mathrm{LS}_{\mathrm{S4}}$ = Structural load station
$M_{\mathrm{xb}}^{\mathrm{LS_1}}, \hat{M}_{\mathrm{xb,EKF}}^{\mathrm{LS_1}}$ = Measured and estimated bending moment at load station 1
P_k^-, P_k = A priori and a posteriori error covariance
Q, R = Process error and measurement noise covariance
V_{A}, V_{W} = Airspeed, Wind speed
X_0 = Flow-separation point
$\alpha_{\mathrm{eff}}, \alpha$ = (Effective) angle of attack
$\delta_{\mathrm{a1}}, \delta_{\mathrm{a2}}$ = Aileron control surface deflections
$\delta_{\mathrm{f1}}, \delta_{\mathrm{f2}}$ = Flaperon control surface deflections
ζ = Modal damping ratio
$\eta, \dot{\eta}, \ddot{\eta}$ = Generalized displacement coordinate and derivatives
μ = Generalized mass
μ, μ_{r} = Mean value
ξ = Damping ratio
σ_{r} = Standard deviation
$\tilde{\phi}_x, p_x$ = Measured Euler angles and angular rates at station x
ω_n = Natural frequency
$\boldsymbol{\Theta}$ = Parameter vector
Φ_η = Mode shape
$\boldsymbol{\Phi}$ = Local model network input vector
$\Phi_{\mathrm{max}}, \Phi_{\mathrm{min}}$ = Maximum and minimum measured roll angle

1 Introduction

Efforts to improve the efficiency of future aircraft configurations have led to the design of increasingly lightweight aircraft wing structures with simultaneously increasing aspect ratios, resulting in higher structural flexibility. Concurrently, these structures are more vulnerable to maneuver and gust loads, necessitating the deployment of active load alleviation systems to further optimize the wing structures' weight [1] to reduce load peaks. However, central to its success is the correct assessment of the aircraft's load condition, achievable through either measurement- or model-based methods. While measurement methods inherently increase system complexity and maintenance effort through additional required load sensors, model-based methods are characterized by high availability and accuracy. In this regard, the Institute of Aircraft Systems Engineering at Hamburg University of Technology (TUHH) has developed a hybrid load monitoring concept named the "hybrid load observer" (LORAS-Hybrid) [2–4]. In essence, the observer combines a physical, model-based observer and a data-driven correction model based on the local model network approach [5]. In its original form, the load observer relies on a Luenberger observer employing a non-linear flight dynamics model [2, 6]. However, the complexity of this model often hinders real-time applications and thus its usage for modern active load alleviation concepts. Facing these limitations, recent work by LUDERER [7, 8] explores the usage of linear parameter-varying (LPV) system-based observers instead of the full non-linear model in wind tunnel experiments. In this context, the LPV extended Kalman filter (LPV-EKF) demonstrates favorable properties in terms of load estimation accuracy and due to its ability to estimate unknown states. In the context of aeroelastic and load control, works by HERRMANN [9] and RIECK [10, 11] leverage these properties, using an LPV-EKF based on validated and refined models to concurrently estimate loads and aeroelastic states. In contrast, LUDERER [8] demonstrated the effectiveness of the hybrid load observer's correction model to compensate for load estimation errors from unvalidated design models. As such, the hybrid load observer is particularly effective when the underlying physical relationships are not immediately apparent or can only be represented with considerable effort, thereby reducing the effort typically required for model refinement while still providing accurate load estimates for control purposes. However, it has so far only been used for structural load monitoring, thus the impact of the underlying model uncertainties on crucial states for load control (e.g. aeroelastic states) remains pending. Given this unresolved aspect, the present work aims to compare an LPV extended Kalman filter derived from a validated simulation model, which corresponds to the conventional way of observer development, and a hybrid load observer based on an LPV extended Kalman filter from unvalidated design models. In doing so, the impact of model fidelity with respect to combined state and load estimation performance can be assessed, which is especially relevant when considering the application of the observer in the context of safety-critical control systems. To this end, both observers are compared to wind tunnel results of a flexible test wing. They differ in terms of the accuracy of their underlying physical models, meaning that one leverages wind tunnel data for model refinement via parameter estimation, while the other relies solely on unvalidated design models. The extension to a hybrid observer and thus the correction model is only applied for the observer based on design models.

This paper is structured as follows. In section 2, the flexible test wing and LPV Extended Kalman filters underlying physical model is presented. To this end, an aeroelastic simulation model based on elastic strip theory and modular subsystems using the in-house library FLYSIM is employed. Its initial parameterization is derived through vortex-lattice aerodynamic calculations, thereby yielding the design model examined in this paper. In addition, a refined, high-fidelity model is derived through parameter estimation from test data. Based on these models, the LPV-EKFs are designed in section 3. Furthermore, a description of the LPV hybrid load observer concept is given. Finally, both LPV observers are assessed and compared in scenario-based wind tunnel tests of a flexible test wing with variable pitch control in section 4.

2 Flexible Wing Model

The unmanned Dimona high aspect-ratio reference aircraft (cf. Figure 1) serves as a test platform for the development and validation of advanced methods for flexible aircraft modeling [9, 12, 13], load estimation [14], and control [10, 15]. In this work, a flexible test wing of the aircraft [14] is employed to investigate the impact of model fidelity on the state and load estimation result of the LPV hybrid load observer in wind tunnel tests. In this regard, this chapter introduces an aeroelastic simulation model based on two different parameterizations, resulting in a *design model* and a *refined model* obtained from parameter estimation and wind tunnel data.

Fig. 1 Dimona reference aircraft

2.1 Flexible Test Wing

The flexible test wing has a span of 2.5 m and a wing area of 0.76 m^2. It features four trailing edge control surfaces, including two flaperons (δ_{f1}, δ_{f2}) located on the inboard sections of the wing, and two ailerons (δ_{a1}, δ_{a2}) on the outboard sections. The test wing is instrumented with strain gauges at the load stations $\mathrm{LS}_{\mathrm{S1}}$ to $\mathrm{LS}_{\mathrm{S4}}$ (cf. Figure 2). These strain gauges are calibrated to measure local structural loads in terms of bending moment, torsion moment, and shear forces. Additionally, five inertial measurement units (IMUs) at the stations $\mathrm{LS}_{\mathrm{I1}}$ to $\mathrm{LS}_{\mathrm{I5}}$ are distributed along the spar to obtain measurements of local accelerations, angular velocities, and Euler angles. These sensor positions are depicted in Figure 2. Note that the observer will rely solely on IMU $\mathrm{LS}_{\mathrm{I5}}$ measurements, while the local load measurements obtained from the strain gauges are used only for model validation and the correction model design.

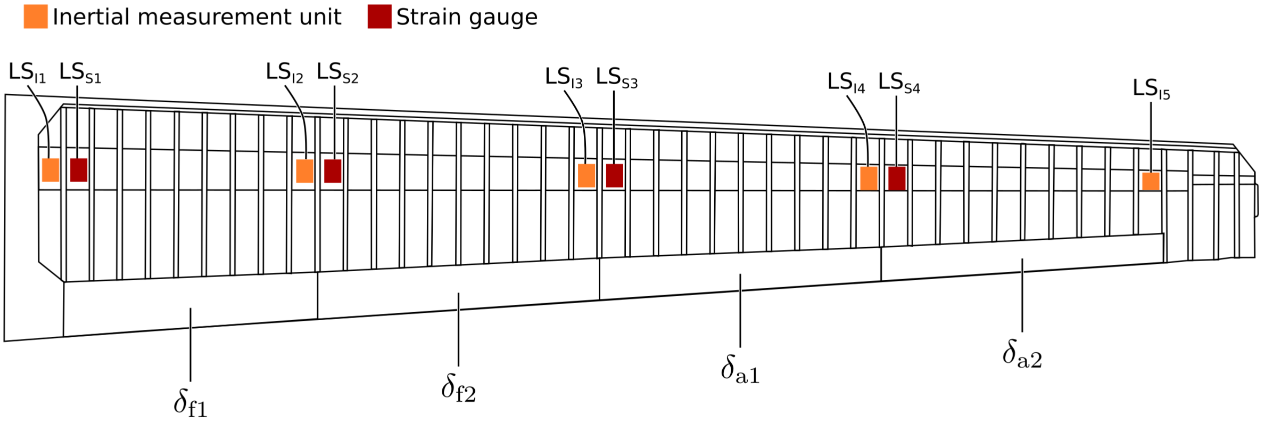

Fig. 2 Measurement stations along the wing

2.2 Aeroelastic Simulation Model

The aeroelastic wind tunnel model for the study conducted in this paper is the non-linear model of the flexible test wing, as presented in [11]. It is implemented in Matlab/Simulink and follows the modular subsystem-based modeling approach of the in-house library FLYSIM. An overview of the aeroelastic model is given in Figure 3.

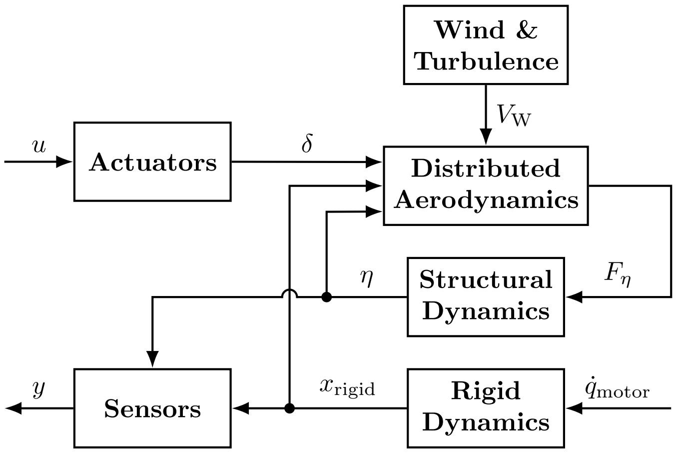

Fig. 3 Overview of the aeroelastic wind tunnel simulation model according to [11]

2.2.1 *Equations of Motion*

Assuming the wind tunnel is operated at a fixed airspeed, the simplified rigid-body dynamics are solely driven by the pitch motor, resulting in the simplified rigid-body dynamics

$$\begin{bmatrix} \dot{u} \\ \dot{v} \end{bmatrix} = \begin{bmatrix} -q\,w \\ q\,u \end{bmatrix} \tag{1}$$

$$\dot{q} = \dot{q}_\mathrm{motor}\,. \tag{2}$$

The aeroelastic equations of motion in modal form, describing the interconnection between the aerodynamics and the structural dynamics, are given as

$$\ddot{\eta}_j + 2\,\zeta_j\,\omega_{n,j}\,\dot{\eta}_j + \omega_{n,j}^2\,\eta_j = \frac{1}{\mu_j}\,F_{\eta_j}. \tag{3}$$

Here, η_j denotes the generalized displacement coordinate, $\omega_{n,j}$ the natural frequency, ζ_j the modal damping ratio, μ_j the generalized mass, and F_{η_j} the generalized force of each mode. The structural dynamics model of the flexible test wing is based on the reference aircraft model by retaining only the symmetric wing modes, as these are decisive for the resulting half-model of a single wing. The original model was obtained based on modal analysis and ground vibration tests [16]. The remaining modes are listed in Table 2 with their respective frequency f and modal damping ξ.

Table 2 First four structural modes of the Dimona test wing according to [11]

Mode	Description	f in Hz	ξ in %
1	1st bending	3.97	0.85
2	In-plane bending	13.21	1.83
3	2nd bending	14.60	1.79
4	Torsion	25.83	1.91

2.2.2 *Distributed Aerodynamics*

The distributed aerodynamics are based on strip theory according to a formulation developed in [9, 12]. A detailed description of this adapted model is provided in [11]. According to strip theory, the wing is discretized into a finite number of spanwise strips (cf. Figure 4). Each strip is assigned local non-dimensional lift and drag coefficients including angle of attack and control surface stall models to describe its aerodynamic characteristics (cf. Equation 4 to 5).

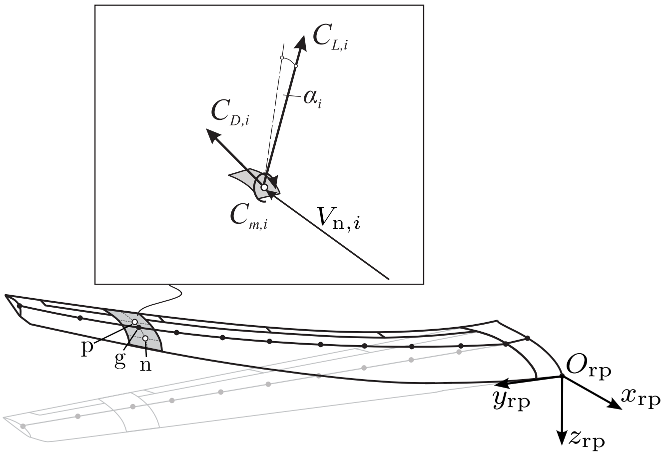

Fig. 4 Aerodynamic properties of the i'th aerodynamic strip on a deformed wing according to [11]

$$\begin{aligned} C_{L,i} &= C_{L_{0},i} + C_{L_{\alpha},i} \cdot \left(\frac{1+\sqrt{X_{0\alpha,i}}}{2} \right)^2 \cdot \alpha_{\text{eff},i} \\ &\quad + \sum_{j=1}^{n_\delta} C_{L_{\delta_j},i} \cdot \left(\frac{1+\sqrt{X_{0\delta,i}}}{2} \right)^2 \cdot \delta_j \end{aligned} \tag{4}$$

$$C_{D,i} = C_{D_{0},i} + k_i \cdot C_{L,i}^2 \,. \tag{5}$$

Here, quasi-steady stall effects are modeled by approximating the steady flow-separation point $X_{0,i}$ [17]. After transferring all coefficients to their respective neutral points, the local forces and moments can be determined based on the local flow conditions that are influenced by the rigid-body motion, structural dynamics, and wind (cf. Equation 3). Based on these distributed forces and moments, the structural loads and the generalized forces of the structural dynamics are determined.

2.3 Model Parametrization

Two models of different fidelity are derived, both using the presented aeroelastic simulation model, but differing with respect to model parametrization. The model structure remains unchanged. The design model is parametrized using baseline stability and control derivative distributions from vortex lattice method (VLM) calculations in XFLR5 (Figure 5a & 5b) and an initial structural-dynamic model (Figure 5c), which represents the wing of the full-aircraft configuration.

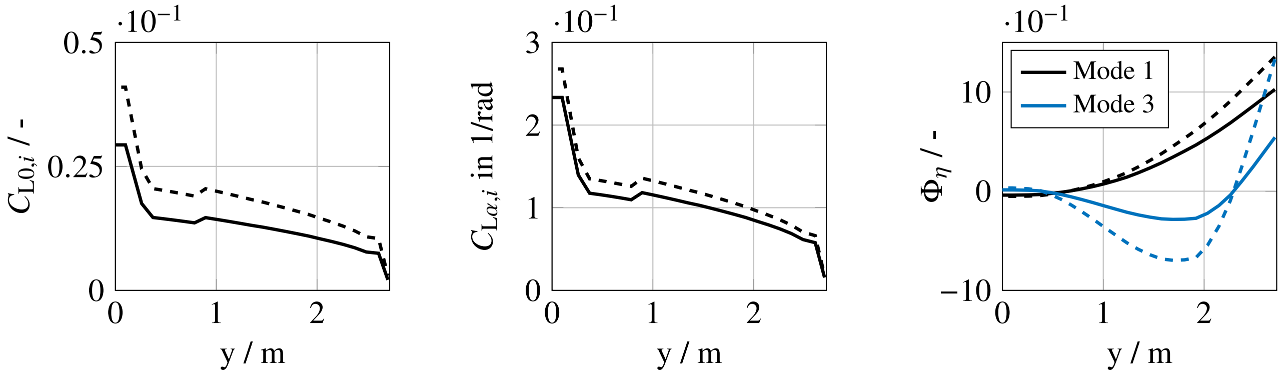

(a) Zero lift: C_{L0}

(b) Lift curve slope: $C_{L\alpha}$

(c) Mode shape: Φ_η

Fig. 5 Comparison of refined (—, —) and design model (- -, - -) parametrization

The refined model is derived through parameter estimation based on the wind tunnel test data defined in Table 4. To this end, the aerodynamic and structural dynamics parameters used in the design model are updated using an output error method [17, 18], optimization of the likelihood function based on a damped Gauss-Newton algorithm, and by employing the DAVIS tool [9, 19]. In this way, the distributions of the aerodynamic coefficients are scaled to match the test data. In addition, the elastic mode shapes are adapted to represent the clamped-wing boundary condition of the wind tunnel. Additionally, parameters of the stall model, actuator model, and sensor model are determined, which is described in detail in [11].

3 LPV Hybrid Load Observer

The hybrid load observer leverages the advantages of two state-of-the-art load monitoring methods by combining a model-based load observer and a data-driven correction model (cf. Figure 6). While both methods individually are capable of structural load estimation, their combination was shown to result in a more pronounced multi-criteria improvement in estimation quality in previous studies [2, 4, 8]. In its original form, the load observer relies on a Luenberger observer [2, 6], which provides a physical estimation of maneuver and gust loads using feedback loops and employing a non-linear flight dynamics model. In this work, the Luenberger observer is substituted with a computationally efficient linear parameter-varying system-based extended Kalman filter (LPV-EKF), as shown in Figure 6. As such, the observer provides model-based estimates of maneuver loads. Moreover, the physical model allows for the estimation of unknown or non-measurable states, such as elastic states or gust velocities, thereby enabling the estimation of gust loads and structural modes. The hybrid load observer's correction model compensates for any load estimation errors, resulting from model approximation errors or neglected physical effects. To this end, a data-driven correction model based on the local-model-network method [20] is employed, which acts as a delta model to the load estimate output of the Kalman filter. Note that, in this work, this correction model is only applied to the LPV extended Kalman filter that is based on design models. Moreover, a purely data-driven method for load and state estimation is not considered, as the advantages of a physical model have already been demonstrated in comparative studies [2, 8].

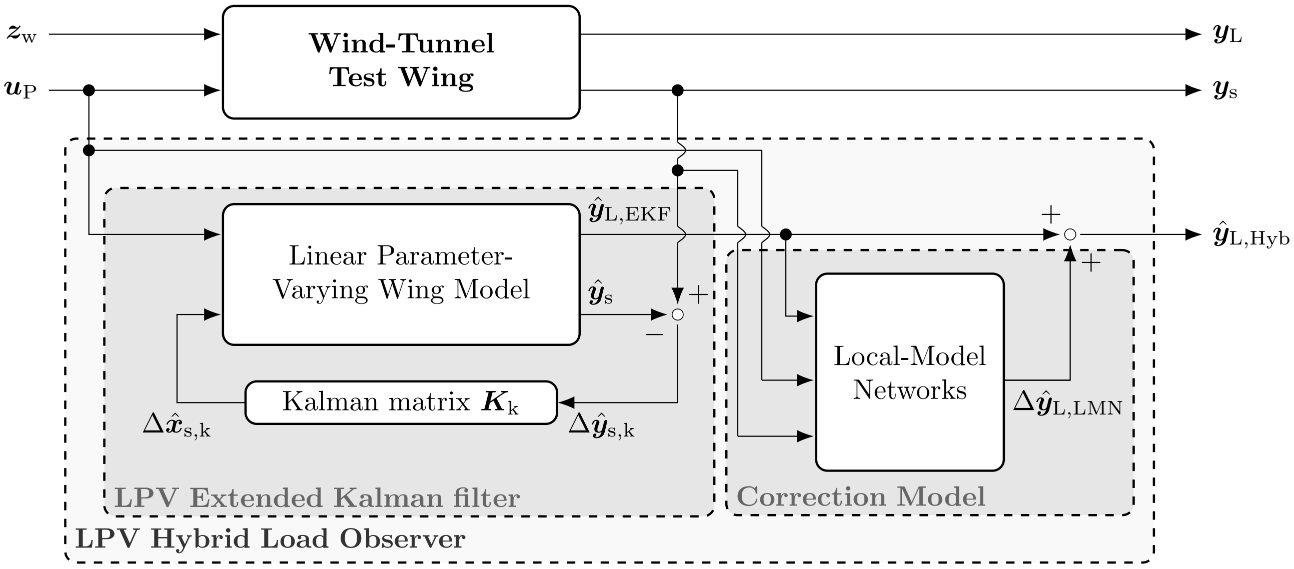

Fig. 6 LPV Extended Kalman filter based hybrid load observer according to [8]

3.1 LPV Extended Kalman Filter

An LPV Extended Kalman filter is employed for load and state estimation. Based on the design and refined model, two extended Kalman filters are designed: A ***Baseline Kalman filter*** based on the design model and a ***Refined Kalman filter*** based on the refined model. Both observers estimate the modal coordinates of the structural dynamics and the wing root bending moment of the test wing, both needed as inputs for e.g. model predictive load control [11]. The Kalman filters use measurements of angle of attack, wind tunnel airspeed, control surface deflections, and IMU bank angle and roll rate at station $\mathrm{LS}_{\mathrm{I5}}$, forming the measurement output vector of the observers.

$$y = \left[u\,, w\,, \delta_{\mathrm{f1}}\,, \delta_{\mathrm{f2}}\,, \delta_{\mathrm{a1}}\,, \delta_{\mathrm{a2}}\,, \tilde{\phi}_5\,, p_5\right]^{\mathsf{T}}$$

Typically used vertical acceleration measurements from the IMUs are excluded due to their comparable lower signal-to-noise ratio in the wind-tunnel tests, which would otherwise increase estimation uncertainties (cf. Rieck [11]). Consequently, the Kalman filters rely only on the local roll rate, which is correlated with $\dot{\eta}_1$, and the local bank angle, which is correlated with η_1 of the first wing bending mode. The linear models for the Kalman filters are obtained from the LPV model depending on the current airspeed, which acts as a scheduling parameter of the grid-based LPV model, as shown in Figure 7.

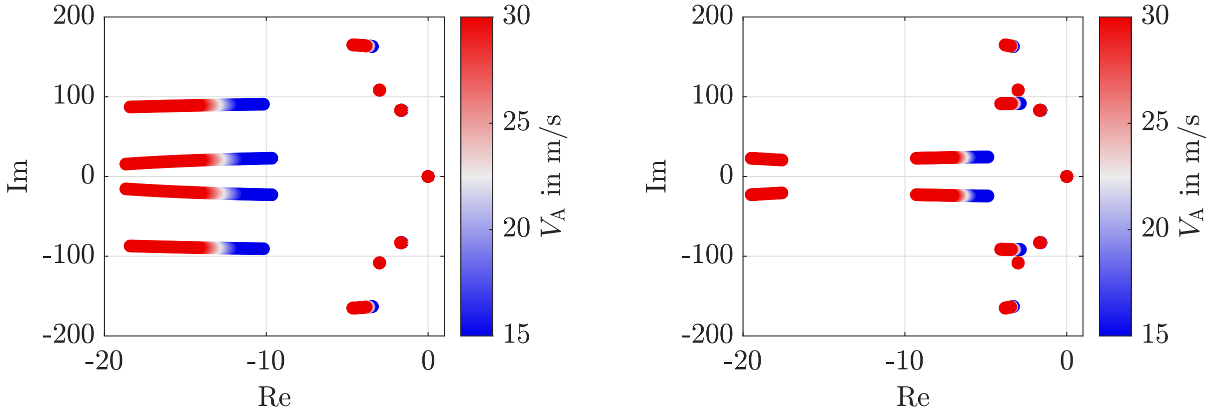

(a) Design Model **(b) Refined Model**

Fig. 7 Comparison of the linearized models used in the LPV systems at varying airspeeds

The prediction step of the Kalman filter is given by Equation 6, where $\hat{x}_k^-$ and P_k^- denote the *a priori* estimates of the states and the error covariance.

$$\begin{aligned} \hat{x}_k^- &= A\,\hat{\tilde{x}}_{k-1} + B\,\tilde{u}_{k-1} + \bar{x} \\ P_k^- &= A\,P_{k-1}\,A^{\mathsf{T}} + Q\,, \end{aligned} \tag{6}$$

The correction step is given by Equation 7, where $\hat{x}_k$ and P_k denote the *a posteriori* estimates.

$$\begin{aligned} K_k &= P_k^-\,C^{\mathsf{T}}\,\left(C\,P_k^-\,C^{\mathsf{T}} + R\right)^{-1} \\ \hat{x}_k &= \hat{x}_k^- + K_k\,\left(y_k - \left(C\,\hat{\tilde{x}}_k^- + D\tilde{u}_k + \bar{y}\right)\right) \\ P_k &= \left(I - K_k\,C\right)\,P_k^-\,, \end{aligned} \tag{7}$$

The loads can then be estimated with the output equation

$$\hat{y}_{L,k} = C^{\mathrm{L}}\,\hat{\tilde{x}}_k + D^{\mathrm{L}}\tilde{u}_k + \bar{y}_{\mathrm{L}}. \tag{8}$$

This process is repeated at each time step, where the matrices of the linear model are updated depending on the current airspeed based on the LPV model.

3.1.1 Observer Design

Both observers are tuned by adjusting the entries of the covariance matrices Q and R. While the noise variances represented by the diagonal entries of the measurement noise covariance R are derived from wind tunnel test data and sensor specifications, the values of Q are obtained using an optimization-based tuning procedure, as proposed in [8, 21]. To this end, the in-house parameter estimation tool DAVIS is employed, thereby determining the diagonal entries of Q with an output error method and maximum-likelihood estimation based on available wind tunnel data. Only the noise variances of the states u, w, q, η_1, and $\dot{\eta}_1$ are estimated, as they are the most sensitive to the optimization target, while all other covariances were fixed at 1e−10. A representative excerpt of the estimation is shown in Figure 8, illustrating the initial observer estimates prior to the *Refined Kalman Filter*'s design and the final estimates obtained after its design. The associated parameter estimation results are summarized in Table 3.

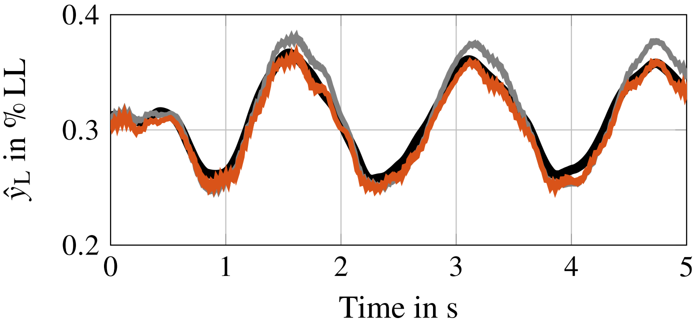

Fig. 8 ***Refined Kalman Filter* design. Wind tunnel (—). Initial estimate (—). Final estimate (—).**

Table 3 Noise variance estimation result

Parameter	Estimate
Q_u	1.60e−3
Q_w	2.14e−5
Q_q	5.19e−6
Q_η	1.53e−7
Q_η	5.03e−3

3.2 Structural Loads Correction Model

The correction model is based on a local-model network, a data-driven method to approximate non-linear relationships by weighted local-linear models (LLM) in simplified subspaces [5]. Specifically, the load correction output, $\Delta\hat{y}_\mathrm{L,LMN}$, is derived by a superposition of local linear function results, $\Delta\hat{y}_{\mathrm{L},i}$, depending on the input vector, $\underline{u}_\mathrm{LMN}$, and the parameter vector $\Theta^{(i)}$. This relationship is summarized in Equation 9 and Equation 10, an overview is given in Figure 9.[1] Each of these LLMs is weighted by a weighting function w_i, assuming a gaussian normal distribution with mean μ, a standard deviation σ and the property $\sum_{\mathrm{i}=1}^{\mathrm{n}} w_i = 1$ (cf. [20]). The correction model design requires experimental data, and is thus subsequently described in section 4.

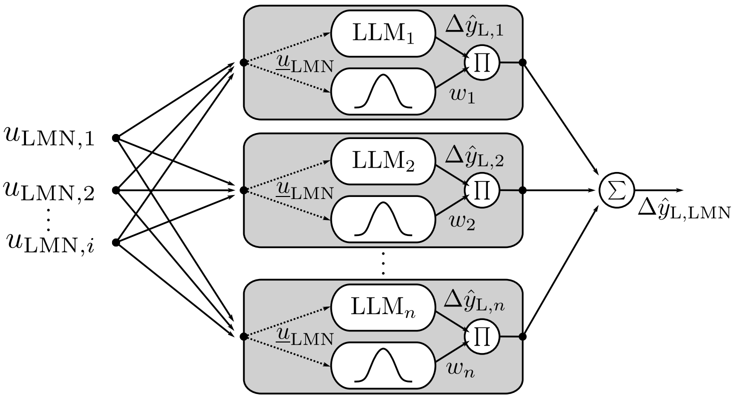

Fig. 9 Structure of a local model network

$$\Delta\hat{y}_\mathrm{L,LMN} = \sum_{i=1}^{\mathrm{n}} w_i(\underline{u}_\mathrm{LMN}, \mu^{(i)}, \sigma^{(i)}) \cdot \Delta\hat{y}_{\mathrm{L},i}(\underline{u}_\mathrm{LMN}, \Theta^{(i)}) \tag{9}$$

$$\begin{aligned}\Delta\hat{y}_{\mathrm{L},i}(\underline{u}_\mathrm{LMN}, \Theta^{(i)}) &= \Phi^T \cdot \Theta^{(i)} \\ &= \begin{bmatrix} 1 & u_\mathrm{LMN,1} & \dots & u_\mathrm{LMN,m} \end{bmatrix}^T \cdot \Theta^{(i)} \\ &= \Theta_0^{(i)} + \Theta_1^{(i)} \cdot u_\mathrm{LMN,1} + \cdots + \Theta_\mathrm{m}^{(i)} \cdot u_\mathrm{LMN,m}\end{aligned} \tag{10}$$

---

[1] Further details are given in [20].

4 Wind tunnel Application and Comparison

In the following, both observers are applied to wind tunnel data of the presented flexible test wing. A scenario-based test procedure is pursued, using conventional system identification maneuvers. A correction model is designed for the *Baseline Kalman filter*, thereby extending the physical load observer to a hybrid load observer. Both observers are compared with respect to their load and state estimation accuracies. To this end, the accuracy of the wing root bending moment estimate (normalized to the limit load) is evaluated at $\mathrm{LS}_{\mathrm{S1}}$. The state estimation aims to estimate the aeroelastic modes, as these are generally not measurable. To this end, the evaluation is primarily focused on the generalized displacement coordinate η_j, including their derivative $\dot{\eta}_j$, as both are relevant to the control concept presented in [11]. Specifically, the displacement coordinate of mode 1 are evaluated, due to its strong correlation with the bending moment. Note that direct measurements of the modes are not possible. Thus, the rates and Euler angles locally measured by the IMUs are used for the comparison. Here, it is exploited that both quantities are strongly correlated with the desired state variables.

4.1 Test Setup

The test setup follows the framework presented in [4, 7] and is depicted in Figure 10. It features a dynamic wing pitch angle control by a stepper motor and four trailing-edge control surfaces. An end plate is used to approximate effects of the wing-fuselage connection.

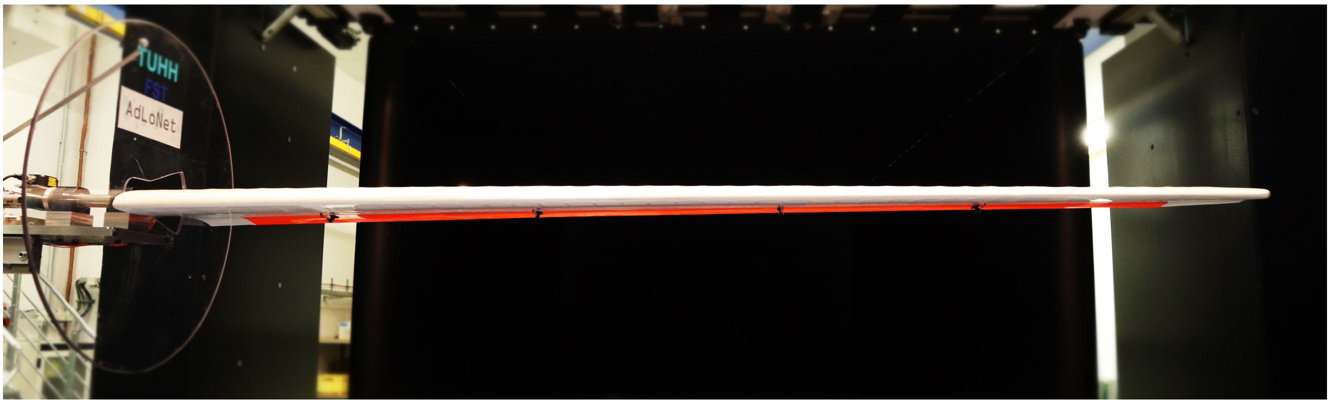

Fig. 10 Experimental set-up of the flexible test wing in the TUHH wind tunnel

The wind tunnel measurement campaign comprises 478 distinct scenarios (Table 4) inspired by conventional system identification maneuvers, following a scenario-based test procedure (cf. Figure 11). The test procedure consists of four consecutive steps, including the maneuver phase during which the actual maneuver is executed. These maneuvers are based on rigid body maneuvers to excite high structural loads and are simulated in advance using the presented flexible wing model (cf. section 2).

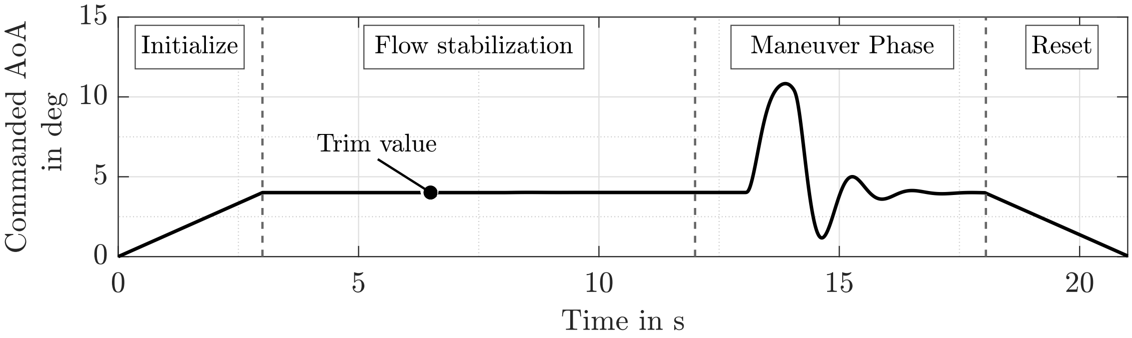

Fig. 11 Scenario-based test procedure according to [8]

All relevant input and output variables of the simulation (e.g. control surface deflections, angle of attack) are recorded and used as input variables for the wing and pitch control in the wind tunnel. The following maneuver types are considered: dynamic angle-of-attack variations (SPM), flap- (FRD) and aileron-doublets (ARD), angle-of-attack- (SPS), flap- (FRS) and aileron-sine excitations (ARS), and combined maneuvers (HGR, simultaneous angle-of-attack and control surface excitation). For the design of the correction model, the database is separated into a training (58 manually selected maneuvers) and validation data set (full database). Moreover, 28 maneuvers are used for the model refinement in section 2. All maneuvers are performed in the airspeed range from $V_A = 16$ to $25\,\mathrm{m\,s^{-1}}$ at varying control surface deflections. All relevant measurement variables are acquired by a real-time measurement system from *dSPACE*. This includes the measured structural loads from strain gauges (bending moment, torsional moment, and shear forces), airspeed data, and the angle-of-attack.

Table 4 Training and validation maneuvers

Type	# of Maneuvers		
	Refined	Training	Validation
ARD	8	15	69
ARS	--	--	36
FRD	10	10	156
FRS	--	--	36
HGR	--	30	43
SPM	6	--	79
SPS	4	3	59
Total	**28**	**58**	**478**

4.2 Correction Model Design

A correction model is designed for the *Baseline Kalman filter*, thereby facilitating a meaningful comparison of both approaches during experimental validation. To this end, the data-driven correction model is derived using the SIGMA tool [20] using the defined training data (Table 4). According to its definition, the correction model acts as a delta model by adding a correction term to the Kalman filter's load estimate. Thus, the difference between the measured and estimated bending moment is used as the target criterion, Y, (cf. Equation 11). A detailed description of the design process can be found in [4, 20].

$$Y = y_L - \hat{y}_{L,EKF} = M_{xb}^{LS_1} - \hat{M}_{xb,EKF}^{LS_1} \tag{11}$$

The input vector is defined as follows:

$$u_{LMN} = \left[u\,,w\,,q\,,\dot{q}\,,\delta_{f1}\,,\delta_{f2}\,,\delta_{a1}\,,\delta_{a2}\,,\hat{M}_{xb,EKF}^{LS_1}\right] \tag{12}$$

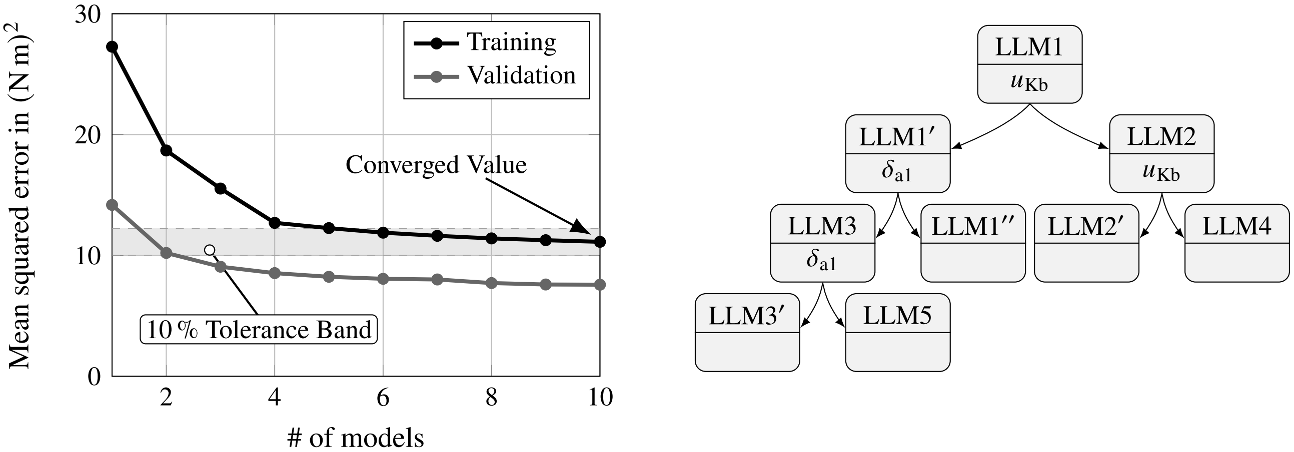

(a) Estimation error with increasing submodels

(b) Correction model structure

Fig. 12 Correction model design

Figure 12a shows how the estimation error evolves with increasing correction model complexity. Accordingly, the design was restricted to five submodels, providing a sufficient compromise between accuracy and complexity of the correction model. The resulting structure is depicted in Figure 12b based on a typical model tree and essentially shows a dependence on the wind tunnel airspeed.

4.3 Load Estimation

The hybrid load observer was developed in the context of structural load monitoring. As such, precise load estimation results are realized even at pronounced modeling errors of the underlying physical model. In this regard, the correction model is a key contributor, which ensures the observer's accuracy even at underlying low physical model fidelity. This property is demonstrated in Figure 13a, where the hybrid observer's bending moment load estimation results and those of the *Baseline Kalman filter* are compared to wind tunnel data. Specifically, the Kalman filter's mean estimation error of 7.3 % LL, the maximum error of 20.9 % LL, and the standard deviation of 2.5 % LL are effectively reduced to 0.1 % LL, 6.3 % LL and 0.8 % LL, which is depicted in Figure 13a.

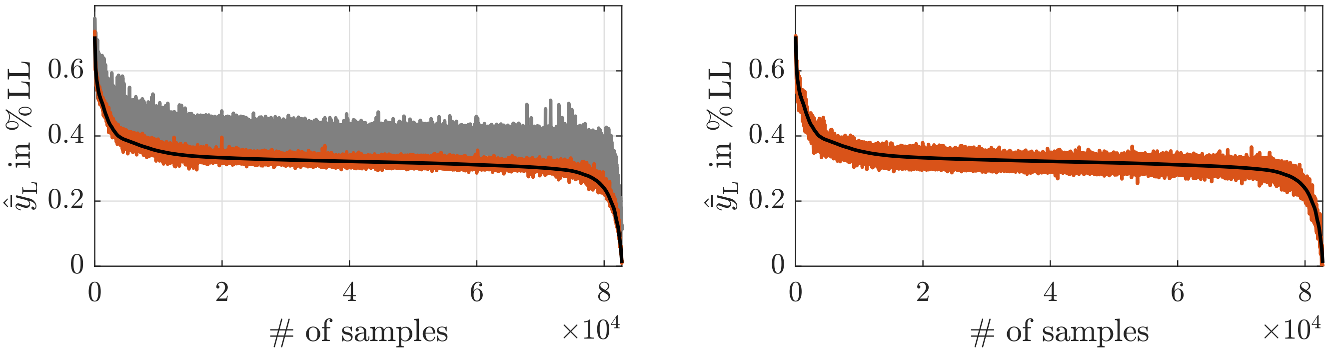

(a) Design model. ***Hybrid Load Observer*** **(—).** ***Baseline Kalman filter*** **(—). Wind tunnel (—).**

(b) Refined model. ***Refined Kalman filter*** **(—). Wind tunnel (—).**

Fig. 13 Comparison of bending moment load estimation results

In contrast, the *Refined Kalman filter* is effective without additional correction (cf. Figure 13b), thereby achieving a mean error of −0.6 % LL, a maximum error of 7.3 % LL and a standard deviation of 1.3 % LL. Although this Kalman filter achieves excellent results, it is still surpassed in terms of load estimation accuracy by the *Hybrid Load Observer* that is based on design models. Here, the correction model contributes to a narrower spread, lower mean errors, and improved accuracy at high loads. A time-domain comparison of an SPM maneuver in Figure 14 reveals two main aspects. First, the *Baseline Kalman filter* exhibits a larger phase shift than the *Refined Kalman filter*. Second, the low delay of the angle-of-attack (AoA) measurement positively affects the time-domain performance of the correction model, reducing the overall delay of the *Hybrid Load Observer* and leading to a slight improvement over the *Refined Kalman filter* for its parameterization considered in this study. The result underscores why hybrid approaches have proven promising for structural load monitoring in previous works [2, 7, 8]. Based on these results, the following conclusions can be drawn:

Table 5 Observer estimation results in % LL

	EKF (Design)	Hybrid (Design)	EKF (Refined)
μ_{r}	7.3	0.1	-0.6
$\lvert r\rvert_{\max}$	20.9	6.3	7.3
σ_{r}	2.5	0.8	1.3

1) The employed correction model effectively compensates for load estimation errors of the Kalman filter that is based on design models.

2) The resulting *Hybrid Load Observer* achieves higher load estimation accuracies than the *Refined Kalman filter*, despite its reduced physical model fidelity.

Based on these findings, it is expected that the correction model can further enhance the *Refined Kalman filter*'s performance. Thus, in terms of load estimation performance, a hybrid approach is preferable, particularly when not all physical relationships are apparent, making a refined model difficult to obtain. Note that the correction model design requires in the present work a larger number of test data compared to the model refinement (cf. Table 4). Consequently, the effort required to train the correction model must be weighed against the effort required to refine the model in practical applications. If data for the correction model design are not available, the *Refined Kalman filter* still demonstrates excellent results.

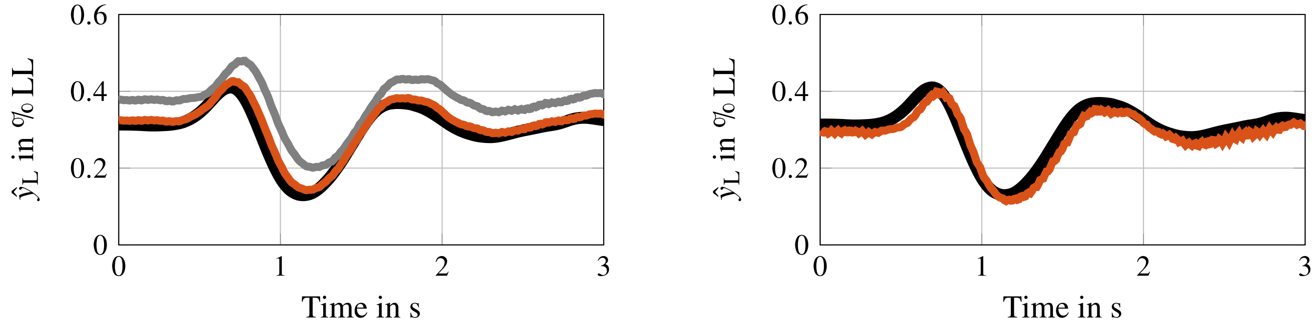

(a) Design model. ***Hybrid Load Observer*** **(—).** ***Baseline Kalman filter*** **(—). Wind tunnel (—).**

(b) Refined model. ***Refined Kalman filter*** **(—). Wind tunnel (—).**

Fig. 14 Time-domain comparison of an SPM maneuver

4.4 Structural Mode Estimation

Table 6 Extreme values of the IMU measurements

	Roll angle in °		Roll rate in ° s^{-1}	
	Φ_{max}	Φ_{min}	p_{max}	p_{min}
LS_{I1}	-0.3	-2.0	5.8	-5.0
LS_{I2}	-0.3	-3.7	11.8	-10.6
LS_{I3}	-0.1	-5.7	19.3	-18.3
LS_{I4}	-0.1	-7.7	27.2	-26.3
LS_{I5}	-0.3	-8.8	35.1	-33.1

In view of both observers' application in modern load control concepts (e.g. [11]), their structural mode estimation accuracies are another crucial performance aspect. In this regard, the generalized coordinate of the first bending mode is of particular interest, as it is the dominant mode of the considered flexible test wing and it correlates with the bending moment evaluated in subsection 4.3. Direct measurements of the modes are challenging to obtain, so that measured roll rates ($p_{LS_{I1}}$ - $p_{LS_{I5}}$) and Euler angles ($\Phi_{LS_{I1}}$ - $\Phi_{LS_{I5}}$) of the spanwise distributed IMUs are compared to the Kalman filters' corresponding outputs as a proxy. A comparison between estimated and measured Euler angles is given in Figure 15. The results clearly indicate advantages for the *Refined Kalman filter*, with respect to its mean (Figure 15a) and maximum estimation error (Figure 15b). Specifically, the mean error is consistently near −1.5° between LS_{I1} and LS_{I4}, thereby revealing a small offset associated with the trim values of aeroelastic simulation model. The maximum error of 2.6° exceeds the mean error by only 1.1° that is further confirmed by the small standard deviation in Figure 15c.

In contrast, the mean estimation error of the *Hybrid Load Observer* gradually increases up to approximately −3°, and its maximum error is 4.6°. As measurements at LS_{I5} are used in the measurement output vector of both observers (cf. subsection 3.1), the corresponding mean and maximum errors are comparatively smaller. A comparison of the roll rate estimation errors is presented in Figure 16. Here, the impact of increased uncertainties, such as measurement noise and model uncertainties, becomes apparent, leading to an incremental rise in the error toward the wingtip and generally higher estimation errors for both observers. Again, the *Refined Kalman filter* shows smaller mean errors, maximum errors, and standard deviations than the *Hybrid Load Observer*. For example, the maximum mean error is 17 times lower than that of the *Hybrid Load Observer*, revealing clear limitations resulting from its reduced physical model fidelity.

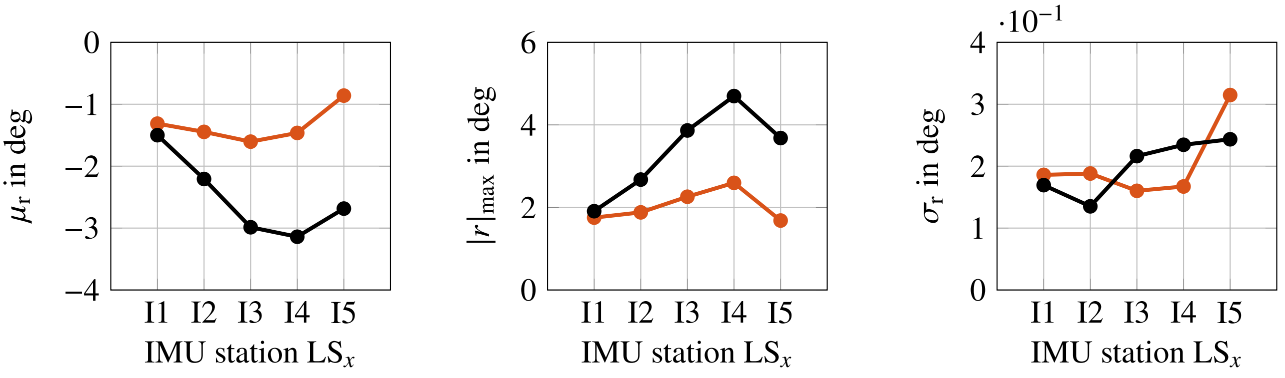

(a) Mean error **(b) Maximum error** **(c) Standard deviation**

Fig. 15 Roll angle estimation error comparison at IMU stations LS_{I1} to LS_{I5}. *Hybrid Load Observer* (●), *Refined Kalman filter* (●).

In conclusion, the demonstrated load estimation accuracy of the *Hybrid Load Observer*, in its current form, is inherently not transferable to its state estimation accuracy. This results from the data-driven correction model only being applied to the structural load output, whereas the state estimation results from the physical observer part only. Naturally, this applies only if the observer's physical model fidelity is low, as examined in this study. In difference, the *Refined Kalman filter* is based on a refined physical model that achieves better state estimation and comparable load estimation accuracies to the *Hybrid Load Observer*.

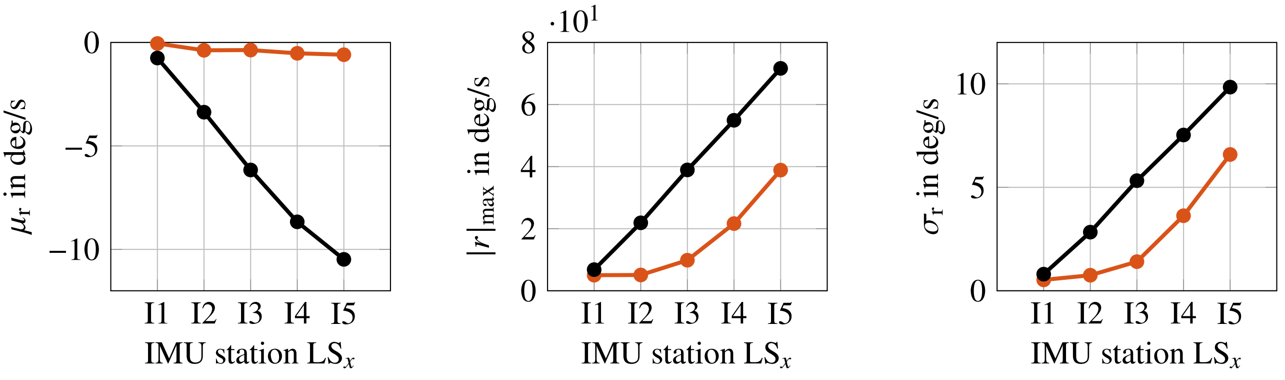

(a) Mean error **(b) Maximum error** **(c) Standard deviation**

Fig. 16 Roll rate estimation error comparison at IMU stations LS_{I1} to LS_{I5}. *Hybrid Load Observer* (●), *Refined Kalman filter* (●).

5 Conclusion

This paper compares two observer methods for structural load and mode estimation with respect to wind tunnel results of a flexible test wing. Specifically, it is focused on the comparison between a hybrid load observer, which combines an LPV-based extended Kalman filter with a data-driven correction model

(*Hybrid Load Observer*), and a purely physical observer based on an LPV-based extended Kalman filter (*Refined Kalman filter*) with previous model refinement. Both concepts are different observer strategies that are connected to individual design complexities. Specifically, the *Hybrid Load Observer* has low development effort on the design models, while requiring a broad data base for model correction. In contrast, the *Refined Kalman filter* relies on elaborate parameter estimation techniques and a suitable data base for model update. However, it avoids the additional complexity of a data-driven correction model. Thus, both of these observers differ in terms of model fidelity and the application of a correction model. As such, they are used to examine the influence of a low-fidelity physical model, refined physical model, and data-driven correction model with respect to the estimation objectives. The comparison clearly shows the advantages of the *Hybrid Load Observer* in terms of load estimation performance, which is higher than that of the *Refined Kalman filter* despite increased model uncertainties. A key factor behind this improvement is that the correction model is specifically trained on measurement data, thus optimizing the hybrid approach for the desired load estimate and surpassing the *Refined Kalman filter*. As such, the *Hybrid Load Observer* demonstrates its effectiveness when the underlying physical model cannot be fully represented while still preserving essential physical relationships. In contrast to previous application of the *Hybrid Load Observer*, where only its load output was relevant, precise estimation of structural modes is desirable for control purposes. In this regard, this work reveals shortcomings in its current implementation if its physical model fidelity is low, due to a single-sided correction of only its load output. This was investigated in the present work by examining the bending mode estimate and its comparison with the measured Euler angles from the wind tunnel tests (correlated with the bending line). The results reveal that although the *Hybrid Load Observer* provides a high load estimation accuracy, it does not achieve the state estimation accuracy of the *Refined Kalman filter* without a correction model. Naturally, this shortcoming could be resolved by improving the fidelity of the underlying physical model. However, if the underlying physical relationships are not apparent, a different type of hybridization in terms of an integrated approach, where also individual state variables of the Kalman filter are corrected, might be an alternative. In addition, it is worth noting that in the present work more measurement data were used to design the correction model than to refine it. It is therefore reasonable to assume that the amount of data required correlates with the model fidelity, highlighting the advantages of a refined physical observer over one that relies heavily on data-driven methods.

Acknowledgments

This work was partly funded by the research project *Integrated flight and loads control of very flexible aircraft for the multidisciplinary aircraft design of future climate-neutral aircraft* (FlexFuture), which is supported by the German Federal Ministry for Economic Affairs and Energy in the national LuFo VI-2 program. Any opinions, findings and conclusions expressed in this document are those of the authors and do not necessarily reflect the views of the other project partners.

Supported by:

Federal Ministry
for Economic Affairs
and Energy

on the basis of a decision
by the German Bundestag

Declaration of Use of Artificial Intelligence

Artificial intelligence was used to refine the language and translation of this work, the authorship remains those of the authors. No parts or entire sections were written by AI.

References

[1] V. Handojo, J. Himisch, K. Bramsiepe, W. R. Krüger, and L. Tichy. Potential estimation of load alleviation and future technologies in reducing aircraft structural mass. *Aerospace*, 9(8), 2022. ISSN: 2226-4310. doi: 10.3390/aerospace9080412.

[2] M. Montel. *Hybride Beobachter-Methode zur Strukturlastüberwachung und deren Validierung mit Flugversuchsdaten*. PhD thesis, Hamburg University of Technology, 2018. Schriftenreihe Flugzeug-Systemtechnik.

[3] M. Montel and F. Thielecke. Efficient and accurate technology for aircraft loads estimation. *CEAS Aeronautical Journal*, 11(2):461–474, 2020. ISSN: 1869-5582. doi: 10.1007/s13272-019-00423-z.

[4] O. Luderer and F. Thielecke. Validation of a Hybrid Loads Observer for a Subscale Test Aircraft with Distributed Electric Propulsion. In *33rd Congress of the International Council of the Aeronautical Sciences ICAS*, page 16, Stockholm, Sweden, 2022. International Council of the Aeronautical Sciences.

[5] M. Halle and F. Thielecke. Local model networks applied to flight loads estimation. In *31st Congress of the International Council of the Aeronautical Sciences ICAS*, page 10, Belo Horizonte, Brazil, 2018. International Council of the Aeronautical Sciences. ISBN: 978-3-932182-88-4.

[6] H. Henrichfreise, L. Bensch, J. Jusseit, L. Merz, and M. Gojny. Estimation of gusts and structural loads for commercial aircraft. In *International Forum on Aeroelasticity and Structural Dynamics (IFASD), Seattle*, 2009.

[7] O. Luderer and F. Thielecke. Aircraft load estimation using linear parameter-varying system-based hybrid observers. *Journal of Aircraft*, 62(3):517–529, 2025. doi: 10.2514/1.C037946.

[8] O. Luderer. *Real-time capable hybrid load observer for aircraft with distributed propulsion*. Phd dissertation, submitted, Hamburg University of Technology, 2026. In review.

[9] B. Herrmann, J. Theis, and F. Thielecke. Nonlinear system identification of a UAV model with distributed aerodynamics and flexible structure. *CEAS Aeronautical Journal*, 2023. doi: 10.1007/s13272-023-00674-x.

[10] L. Rieck, B. Herrmann, F. Thielecke, and H. Werner. Efficient Quasi-Linear Model Predictive Control of a Flexible Aircraft Based on Laguerre Functions. In *American Control Conference ACC*, pages 2855–2860, San Diego, CA, USA, 2023. doi: 10.23919/ACC55779.2023.10156329.

[11] L. Rieck, B. Herrmann, O. Luderer, and F. Thielecke. Model predictive gust load alleviation for a flexible wing considering system limitations. Manuscript in review, presented at DLRK 2025, 2025.

[12] B. Herrmann, J. Theis, and F. Thielecke. System Identification of a Nonlinear UAV Model with Distributed Aerodynamics and Flexible Structure. In *6th Conference on Guidance, Navigation and Control CEAS*, 2022.

[13] L. Rieck, B. Herrmann, and F. Thielecke. Doublet lattice modeling and analysis of unsteady aerodynamic effects for a flexible unmanned aircraft during maneuvers and gust encounters. In *International Forum on Aeroelasticity and Structural Dynamics, IFASD 2024*, 2024.

[14] Oliver Luderer and Frank Thielecke. Development and Testing of a Complementary Sensor Network for Robust Estimation of Maneuver and Gust Loads. In *Deutscher Luft- und Raumfahrtkongress DLRK*, page 12. Deutsche Gesellschaft für Luft- und Raumfahrt - Lilienthal-Oberth e.V., 2023. doi: 10.25967/610085.

[15] B. Herrmann, L. Rieck, and F. Thielecke. Flight testing of real-time model predictive flight control for unmanned flexible aircraft. In *Proceedings of the 2024 CEAS EuroGNC conference*, Bristol, UK, June 2024. doi: 10.82124/CEAS-GNC-2024-054.

[16] K. Henning, M. Montel, A. Köthe, F. Thielecke, and R. Luckner. Experimentelle ermittlung der modalen strukturparameter eines skalierten flugversuchsträgers mittels low-cost sensoren. In *Deutscher Luft-und Raumfahrtkongress DLRK*, 2017.

[17] R. V. Jategaonkar. *Flight Vehicle System Identification: A Time-Domain Methodology, Second Edition*, volume 82. American Institute of Aeronautics and Astronautics, Inc, Reston, VA, 2015. ISBN: 978-1-62410-278-3. doi: 10.2514/4.102790.

[18] V. Klein and E.A. Morelli. *Aircraft System Identification: Theory and Practice*. AIAA education series. American Institute of Aeronautics and Astronautics, 2006. ISBN: 9781563478321.

[19] M. Krings and F. Thielecke. A predictive envelope protection system using linear, parameter-varying models. *CEAS Aeronautical Journal*, 6(1):95–108, 2014. ISSN: 1869-5590. doi: 10.1007/s13272-014-0129-9.

[20] M. Halle. *Lokalmodell-Netz-Identifikation als Analyse- und Bewertungsmethodik von Flugmanoeverlasten*. PhD thesis, Hamburg University of Technology, 2016. Schriftenreihe Flugzeug-Systemtechnik.

[21] J. A. Grauer and E. A. Morelli. Aircraft parameter estimation considering process and measurement noise. *Journal of Aircraft*, pages 1–12, 2024. ISSN: 1533-3868. doi: 10.2514/1.c038080.